Approximate Godunov-Suliciu Scheme for the Seven-Equations Two-Phase Flow Model

P. Richter[a]

[a]*Karlsruhe Institute of Technology (KIT), Steinbuch Centre for Computing, Hermann-von-Helmholtz-Platz 1, 76344 Eggenstein-Leopoldshafen, Germany*

Abstract

The numerical computation of two-phase flows can be described with a Baer-Nunziato type PDE system. Within this work closure laws for interfacial velocity and interfacial pressure are proposed such that the interfacial contact discontinuity is associated with a linearly degenerate field. The resulting two-velocity two-pressure seven-equations model is hyperbolic, consistent with the second law of thermodynamics, fulfills the non-resonance condition and is symmetrizable. Because the system is in non-conservative form, appropriate numerical solvers have to be developed which find the physically relevant solution where the jump conditions are consistent with the viscous profiles. In this work an approximate path-conservative Godunov solver is presented, which uses a Suliciu-relaxation to get a linearly degenerated characteristic field. A solution of the intermediate states of the Riemann problem can be obtained with a careful weakening of the nonlinear Rankine-Hugoniot conditions at the contact discontinuity of the volume fraction. By using the solution of the simplified Riemann invariants, it is ensured that at least six out of eight original Rankine-Hugoniot conditions of the volume fraction are always fulfilled. Within a case study the approximate Godunov-Suliciu solver is tested against several multiphase flow problems, and is compared with a path-conservative entropy-preserving scheme.

Keywords: Two-phase flow, Hyperbolic system, Non-conservative terms, Finite volume method, Suliciu relaxation, Godunov method

1. Introduction

To describe a two-phasic flow in general the conservation of mass, momentum and energy is supposed for both phases. The *homogeneous equilibrium model* [1] is based on the assumption that the two-phase mixture behaves as a single-phase fluid. It uses mean fluid properties that are weighted relatively to vapor and liquid content and it is assumed, that both phases have equal velocities. This model is often used for the description of direct steam generation in a tube [2], [3], [4], [5].

The *separated two-phase flow model* [6] considers the phases to be artificially segregated into a liquid and a vapor stream. Therefore the model bases on a system of six equations – three equations for each phase. These six-equations

*Corresponding author
Email address: pascal.richter@kit.edu (P. Richter)

models are widely used in nuclear thermal-hydraulic codes (RELAP5[1], TRAC[2], CATHARE[3], SPACE[4]). In some recent publications these models from nuclear thermal-hydraulic codes are used [7], [8]. As closure condition, equal pressure in both phases is assumed. Following Saurel and Abgrall [9], this choice yields ill-posed mathematical models and results in numerical instabilities. As extension of the six-equations two-fluid model a Baer Nunziato [10] type partial differential equation system is used. Drew and Passman [11] and Saurel and Abgrall [9] propose the *two-pressure two-phase model*. An additional equation for volume fraction completes the system of equations. This hyperbolic model allows simulations of liquid phase at negative pressure, while the pressure of the vapor phase remains positive, and vice versa. For the underlying problem appropriate numerical solvers have to be developed, as the inhomogeneous model is in non-conservative form, has a low Mach number and stiff source terms [12].

This work is structured as follows. In Section 2 the *two-pressure two-phase model* with its thermodynamic and mathematical properties are introduced. A standard concept for a finite volume scheme which solves the underlying problem is described in Section 3, where the problem is solved using an entropy-preserving path-conservative scheme. In Section 4 an approximate Godunov-type method is developed by finding a Riemann solution of the Suliciu-relaxated model. Both solvers are validated and compared against well-defined test cases in Section 5. In Section 6 we draw a conclusion regarding the presented finite volume methods and give an outlook with possibilities to extend this work.

2. Two-fluid two-pressure model

The *two-velocity two-pressure seven-equations* model from Saurel and Abgrall [9] is generic for all materials or fluids. The model can be written in the general non-conservative form [13],

$$\partial_t \mathbf{u} + \partial_x \mathbf{f}(\mathbf{u}) + B(\mathbf{u})\,\partial_x \mathbf{u} = \mathbf{s}(\mathbf{u}), \tag{1}$$

[1]Reactor Excursion and Leak Analysis Program by Idaho National Laboratory
`www.inl.gov/relap5`.

[2]Transient Reactor Analysis Code by Los Alamos National Laboratory
`nuclear.lanl.gov/nrc.shtml`.

[3]Code for Analysis of Thermalhydraulics during an Accident of Reactor and safety Evaluation by Commisariat á l'Energie Atomique
`www-cathare.cea.fr`.

[4]Safety and Performance Analysis Code by Korea Atomic Energy Research Institute
`www.kaeri.re.kr`.

with state vector $\mathbf{u}$, flux vector $\mathbf{f}(\mathbf{u})$, non-conservative matrix $B(\mathbf{u}) \in \mathbb{R}^{7\times 7}$, and source terms $\mathbf{s}(\mathbf{u})$:

$$\mathbf{u} := \begin{pmatrix} \alpha_1 \\ \alpha_1\rho_1 \\ \alpha_1\rho_1 v_1 \\ \alpha_1\rho_1 E_1 \\ (1-\alpha_1)\rho_2 \\ (1-\alpha_1)\rho_2 v_2 \\ (1-\alpha_1)\rho_2 E_2 \end{pmatrix}, \quad \mathbf{f}(\mathbf{u}) = \begin{pmatrix} 0 \\ \alpha_1\rho_1 v_1 \\ \alpha_1(\rho_1 v_1^2 + p_1) \\ \alpha_1(\rho_1 E_1 + p_1)v_1 \\ (1-\alpha_1)\rho_2 v_2 \\ (1-\alpha_1)(\rho_2 v_2^2 + p_2) \\ (1-\alpha_1)(\rho_2 E_2 + p_2)v_2 \end{pmatrix}, \quad B(\mathbf{u}) = \left(\begin{array}{c:c} v_\mathrm{i} & \\ 0 & \\ -p_\mathrm{i} & \\ -p_\mathrm{i} v_\mathrm{i} & 0 \\ 0 & \\ p_\mathrm{i} & \\ p_\mathrm{i} v_\mathrm{i} & \end{array}\right). \tag{2}$$

All solutions for the state vector $\mathbf{u}$ are in the set of admissible states,

$$\Omega = \{\mathbf{u} \in \mathbb{R}^7 \mid \alpha_1 \in (0,1), \;\; \rho_1, \rho_2, u_1, u_2, c_1, c_2 \in \mathbb{R}^+\}. \tag{3}$$

As parameters we have the density ρ, velocity v, pressure p, specific total energy $E := u + \frac{1}{2}v^2$, and specific internal energy u. The subscripts 1 and 2 describe the two phases (e.g. liquid and gas). The subscript i describes the interfacial property between both phases. So, v_i and p_i describe the velocity and pressure of the phase change between phase 1 and phase 2. The volume fraction α_1 describes the volumetric ratio of the phasic material. To ensure that both phases are always everywhere present, it must hold $\alpha_1 \in (0,1)$. Furthermore, for short notation we define $\alpha_2 := (1-\alpha_1)$. The system (1) is associated with an initial state,

$$\mathbf{u}(t_0, x) = \mathbf{u}_0(x), \quad \mathbf{u}_0(x) \in \Omega \;\;, \;\; x \in \mathbb{R}. \tag{4}$$

For a transformation of the system (1) in a closed quasilinear form,

$$\partial_t \mathbf{u} + A(\mathbf{u})\, \partial_x \mathbf{u} = \mathbf{s}(\mathbf{u}), \tag{5}$$

we need to differentiate the flux vector $\mathbf{f}(\mathbf{u})$ with respect to our independent variables $\mathbf{u}$, such that the system matrix is given by

$$\begin{aligned} A(\mathbf{u}) :=\; & \partial_{\mathbf{u}} \mathbf{f}(\mathbf{u}) + B(\mathbf{u}) \\ = & \begin{pmatrix} v_\mathrm{i} & 0 & 0 & 0 & 0 & 0 & 0 \\ 0 & 0 & 1 & 0 & 0 & 0 & 0 \\ p_1 - p_\mathrm{i} - \rho_1 \cdot (p_1)_\rho & A_{\mathrm{mom},\rho_1} & A_{\mathrm{mom},\rho_1 v_1} & A_{\mathrm{mom},\rho_1 E_1} & 0 & 0 & 0 \\ p_1 v_1 - p_\mathrm{i} v_\mathrm{i} - \rho_1 v_1 \cdot (p_1)_\rho & A_{\mathrm{ener},\rho_1} & A_{\mathrm{ener},\rho_1 v_1} & A_{\mathrm{ener},\rho_1 E_1} & 0 & 0 & 0 \\ 0 & 0 & 0 & 0 & 0 & 1 & 0 \\ -\big(p_2 - p_\mathrm{i} - \rho_2 \cdot (p_2)_\rho\big) & 0 & 0 & 0 & A_{\mathrm{mom},\rho_2} & A_{\mathrm{mom},\rho_2 v_2} & A_{\mathrm{mom},\rho_2 E_2} \\ -\big(p_2 v_2 - p_\mathrm{i} v_\mathrm{i} - \rho_2 v_2 \cdot (p_2)_\rho\big) & 0 & 0 & 0 & A_{\mathrm{ener},\rho_2} & A_{\mathrm{ener},\rho_2 v_2} & A_{\mathrm{ener},\rho_2 E_2} \end{pmatrix} \end{aligned} \tag{6}$$

with phasic parameters $k = 1, 2$, and

$$A_{\mathrm{mom},\rho_k} := -v_k^2 + (p_k)_\rho - (p_k)_u \cdot \frac{E_k - v_k^2}{\rho_k}, \qquad A_{\mathrm{mom},\rho_k v_k} := 2v_k + \frac{-(p_k)_u \cdot v_k}{\rho_k}, \qquad A_{\mathrm{mom},\rho_k E_k} := \frac{(p_k)_u}{\rho_k}$$

$$A_{\mathrm{ener},\rho_k} := v_k \left((p_k)_\rho - (p_k)_u \cdot \frac{E_k - v_k^2}{\rho_k} - \frac{p_k}{\rho_k} - E_k \right), \qquad A_{\mathrm{ener},\rho_k v_k} := E_k + \frac{p_k - (p_k)_u \cdot v_k^2}{\rho_k}, \qquad A_{\mathrm{ener},\rho_k E_k} := v_k + \frac{v_k \cdot (p_k)_u}{\rho_k}.$$

2.1. Closures for the thermodynamic properties

To close the system the phasic density ρ and specific internal energy u are used as intensive properties to provide each phase with thermal properties as equation of state. For a compressible fluid the following stiffened gas equation of state was performed for pressure, temperature, speed of sound and specific Gibbs free energy [14]:

$$\begin{aligned} p(\rho,u) &= (\gamma-1)\rho(u-q)-\gamma\pi, \\ T(\rho,u) &= \frac{1}{c_\mathrm{v}}\left(u-q-\frac{\pi}{\rho}\right), \\ c(\rho,u) &= \sqrt{\gamma\,\frac{p+\pi}{\rho}}, \\ g(\rho,u) &= g(p,T) = (\gamma c_\mathrm{v}-q')T - c_\mathrm{v}T\log\left(\frac{T^\gamma}{(p+\pi)^{\gamma-1}}\right)+q. \end{aligned} \tag{7}$$

The five constants, as $\gamma > 0$, specific heat at constant volume $c_\mathrm{v} \geq 0$, $\pi \geq 0$, binding energy $q \geq 0$, and $q' \geq 0$ are given for each fluid particularly. For a calorically ideal gas the three parameters π, q, and q' are set to zero.

To find closures for the interfacial velocity v_i and interfacial pressure p_i, we derive thermodynamic and mathematical conditions from the model which should be fulfilled. In the following Subsection 2.2 the hyperbolicity of the model is examined, which delivers an additional constraint for the interfacial velocity v_i. This parameter is then closed in Section 2.3 by choosing it in such a way that the v_i-contact discontinuity is associated with a linearly degenerate field. Then in Subsection 2.4 the condition for the validity of the second law of thermodynamics is derived. The entropy compatibility condition delivers a closure for the interfacial pressure p_i. Finally, in Section 2.5 it is verified that the system is symmetrizable.

2.2. Hyperbolicity

Because the model only describes transport effects, it should be hyperbolic to ensure that all wave speeds are finite and the system may be locally decoupled [15]. This is given as soon as the model provides real eigenvalues and the corresponding eigenvectors are linearly independent. Therefore, Gallouët, Hérard and Seguin [16] transformed the system in quasi-conservative form in terms of primitive quantities. The primitive system matrix admits the seven eigenvalues v_i, v_1, v_2, $v_1 \pm c_1$, and $v_2 \pm c_2$, which are all real but not necessarily distinct. All eigenvectors are linearly independent as soon as the v_i-corresponding eigenvector is defined. To avoid that its denominator would become zero the non-resonance condition [17, 15] must hold,

$$v_\mathrm{i} \neq v_1 \pm c_1 \quad \text{and} \quad v_\mathrm{i} \neq v_2 \pm c_2. \tag{8}$$

The interfacial velocity will be chosen below in (10) as convex combination of the phasic velocities, such that $v_\mathrm{i} \in [v_1, v_2]$. For subsonic flows it holds $v_1 \ll c_1$ and $v_2 \ll c_2$, such that the non-resonance condition (8) is fulfilled[5].

[5]The hyperbolicity of the system was also shown in [18], Part II, Section 2.5.2 for the primitive system vector $\tilde{\mathbf{u}} := (\alpha_1, \rho_1, v_1, p_1, \rho_2, v_2, p_2)^\mathsf{T}$.

2.3. Characteristic fields

The solution of the quasilinear system (5) is determined by seven characteristic fields, where each consists of a characteristic speed and a corresponding wave. T.-P. Liu classified the waves of characteristic fields into two different waves: a contact discontinuitiy (*linearly degenerated field*), and a shock or rarefaction wave (*genuinely nonlinear field*) [19]. As known from the Euler equations, just the field associated with the fluid velocity is linearly degenerate, where the other fields are genuinely nonlinear.

The field associated with the eigenvalue v_i depends on the choice of the interfacial velocity v_i. This wave corresponds to the non-conservative term $v_\mathrm{i}\partial_x\alpha_1$ in the volume fraction equation, see first equation of the system (1) with (2). Because the volume fraction α_1 should be preserved through the v_i-contact discontinuity, v_i should be chosen in such a way that this discontinuity is associated with a linearly degenerate field [20].

From a physical point of view it is reasonable to assume the interfacial velocity v_i as a convex combination of the phasic velocities v_1 and v_2 [9, 16], such that we define:

$$v_\mathrm{i} := \beta v_1 + (1-\beta)v_2 \quad \text{with} \quad \beta \in [0,1]. \tag{9}$$

If we now follow Saleh [20] and set β as mass fraction,

$$\beta := \frac{\xi\alpha_1\rho_1}{\xi\alpha_1\rho_1 + (1-\xi)\alpha_2\rho_2} \quad \text{with} \quad \xi \in [0,1], \tag{10}$$

the derivative of the eigenvalue v_i with respect to the primitive variables is orthogonal to its corresponding eigenvector, such that the field of the v_i-wave is linearly degenerate[6]. So, altogether the interfacial velocity is given as

$$v_\mathrm{i} := \frac{(1-\xi)\alpha_1\rho_1 v_1 + \xi\alpha_2\rho_2 v_2}{(1-\xi)\alpha_1\rho_1 + \xi\alpha_2\rho_2} \quad \text{with} \quad \xi \in [0,1]. \tag{11}$$

This formulation is well defined, as all parameters are positive. In literature, mostly the three interfacial velocities,

$$v_\mathrm{i} = v_1, \quad v_\mathrm{i} = v_2, \quad \text{and} \quad v_\mathrm{i} = \frac{\alpha_1\rho_1 v_1 + \alpha_2\rho_2 v_2}{\alpha_1\rho_1 + \alpha_2\rho_2}, \tag{12}$$

are used [21], which correspond to the above defined interfacial velocity with $\xi = 0$, $\xi = 1$, and $\xi = \frac{1}{2}$.

2.4. Second law of thermodynamics

From a physical perspective, a model has to be consistent with the second law of thermodynamics. Therefore, to select the physically relevant entropy solution [22], the entropy inequality is derived and used as additional condition on the constitutive laws. Thus, for Lax's entropy-entropy flux pair (η, ψ) with convex entropy function $\eta(\mathbf{u})$ and its corresponding entropy flux $\psi(\mathbf{u})$ the additional conservation law,

$$\partial_t\eta(\mathbf{u}) + \partial_x\psi(\mathbf{u}) = 0, \tag{13}$$

should hold for for smooth solutions, while for discontinuous solutions $\mathbf{u}$ the above conservation law becomes an inequality,

$$\partial_t\eta(\mathbf{u}) + \partial_x\psi(\mathbf{u}) \leq 0. \tag{14}$$

[6] More details can be found in [18], Part II, Section 2.5.3.

A weak solution is said to be an *entropy solution*, if it satisfies the above inequality in the distributional sense. The entropy flux $\psi(\mathbf{u})$ is chosen such that it satisfies the compatibility condition [23],

$$\partial_{\mathbf{u}}\psi(\mathbf{u})^{\mathsf{T}} \stackrel{!}{=} \partial_{\mathbf{u}}\eta(\mathbf{u})^{\mathsf{T}}\, A(\mathbf{u}). \tag{15}$$

Then the validity of the entropy inequality (14) can directly be derived from the multiplication of the so-called entropy variables $\mathbf{v}(\mathbf{u}) := \partial_{\mathbf{u}}\eta(\mathbf{u})$ and the equation system (5).

Motivated by the thermodynamics of the system, a candidate for an entropy-entropy flux pair for our model is the physical entropy of the mixture,

$$\begin{aligned} \eta(\mathbf{u}) &= -\big(\alpha_1\rho_1 s_1 + \alpha_2\rho_2 s_2\big), \\ \text{and} \quad \psi(\mathbf{u}) &= -\big(\alpha_1\rho_1 v_1 s_1 + \alpha_2\rho_2 v_2 s_2\big), \end{aligned} \tag{16}$$

with specific entropy s, given by its physical law,

$$sT = u + \frac{p}{\rho} - g, \tag{17}$$

where g is the specific Gibbs free energy.

In order to verify that $\eta(\mathbf{u})$ is a convex function of $\mathbf{u}$, we follow the proof of Coquel et al. [17]. The key idea is to at first show that the phasic entropy functions $(-\rho_1 s_1)$ and $(-\rho_2 s_2)$ are strictly convex functions. Then, the convexity of the entropy function can be shown by expressing the entropy function $\eta(\mathbf{u})$ in terms of these stricly convex phasic entropy functions and proving the semi-definiteness of its Hessian[7].

For the chosen entropy-entropy flux pair it remains to show that the entropy function $\eta(\mathbf{u})$ fulfills the compatibility condition (15). With the entropy variables[8],

$$\mathbf{v}(\mathbf{u}) := \partial_{\mathbf{u}}\eta(\mathbf{u}) = \begin{pmatrix} \frac{p_2}{T_2} - \frac{p_1}{T_1} \\ \dfrac{\frac{p_1}{\rho_1} + u_1 - \frac{1}{2}v_1^2}{T_1} - s_1 \\ \frac{v_1}{T_1} \\ -\frac{1}{T_1} \\ \dfrac{\frac{p_2}{\rho_2} + u_2 - \frac{1}{2}v_2^2}{T_2} - s_2 \\ \frac{v_2}{T_2} \\ -\frac{1}{T_2} \end{pmatrix} \stackrel{(17)}{=} \begin{pmatrix} \frac{p_2}{T_2} - \frac{p_1}{T_1} \\ \dfrac{g_1 - \frac{1}{2}v_1^2}{T_1} \\ \frac{v_1}{T_1} \\ -\frac{1}{T_1} \\ \dfrac{g_2 - \frac{1}{2}v_2^2}{T_2} \\ \frac{v_2}{T_2} \\ -\frac{1}{T_2} \end{pmatrix}, \tag{18}$$

the entropy compatibility condition (15) delivers in the first row[9], a condition for the unknown interfacial pressure (while the other six rows are equal):

$$\frac{(p_1 - p_\mathrm{i})(v_1 - v_\mathrm{i})}{T_1} - \frac{(p_2 - p_\mathrm{i})(v_2 - v_\mathrm{i})}{T_2} \;\stackrel{!}{=}\; 0. \tag{19}$$

Substituting the expression for the interfacial velocity in (11), we get for p_i a convex combination of p_2 and p_1,

$$p_\mathrm{i} \;=\; \frac{(1-\xi)\alpha_1\rho_1 T_1\, p_2 + \xi\alpha_2\rho_2 T_2\, p_1}{(1-\xi)\alpha_1\rho_1 T_1 + \xi\alpha_2\rho_2 T_2}, \tag{20}$$

[7] The fully expanded proof for the convexity of the entropy function can be found in [18], Part II, Eq. (2.95)ff.

[8] The partial derivatives of the specific entropy can be found in [18], Part II, Eq. (2.89).

[9] The fully expanded equality of the entropy compatibility can be found in [18], Part II, Eq. (2.93).

which depends on the mass fraction ratio parameter ξ of the interfacial velocity (11). This formulation is well defined, as all parameters are positive.

2.5. Symmetrization of the hyperbolic system

A hyperbolic system should provide the property that locally in time there exists a smooth solution of the corresponding Cauchy problem. Godlewski and Raviart [24] showed that for conservative problem this property comes with the existence of an entropy-entropy flux pair. But for non-conservative problems we additionally need to show that the system is symmetrizable. For two-phase flow this was first proven in [17] and was extended for multi-components fluids in [15]. In both publications a symmetric positive definite matrix was constructed for a different set of primitive variables[10]. Note that the choice for the symmetric positive definite matrix is just realizable if the non-resonance condition (8) holds.

3. Entropy-preserving path-conservative scheme

As the two-phase flow problem (1) consist of a non-conservative part $B(\mathbf{u})\,\partial_x\mathbf{u}$ we can't use the standard finite volume methods. Instead, we follow the idea of path-conservative schemes which uses the formulation in closed quasilinear form (5). The one-dimensional spatial domain is partitioned in a regular mesh of grid cells $C_i := \left(x_{i-1/2},\, x_{i+1/2}\right)$ with the length Δx, while $\Delta t = t^{n+1} - t^n$ denotes the time step at time t^n.

To find an approximated solution $\mathbf{u}_i^{n+1}$ of the Cauchy problem for each cell C_i at time t^{n+1}, we use the *fractional-step* method, where the full problem is divided into two sub-problems, a convective sub-system,

$$\begin{cases} \partial_t\mathbf{u} + A(\mathbf{u})\,\partial_x\mathbf{u} = 0 \quad \text{for} \quad x \in \mathbb{R},\;\; t \in (t^n, t^{n+1}) \\ \mathbf{u}(x, t^n) = \mathbf{u}_i^n \quad \text{for} \quad x \in C_i, \end{cases} \tag{21}$$

which computes the intermediate solution $\mathbf{u}_i^{n+1,-}$ of the convective part, and a relaxation sub-system considering the source terms,

$$\begin{cases} \partial_t\mathbf{u} = \mathbf{s}(\mathbf{u}) \quad \text{for} \quad x \in \mathbb{R},\;\; t \in (t^n, t^{n+1}) \\ \mathbf{u}(x, t^n) = \mathbf{u}_i^{n+1,-} \quad \text{for} \quad x \in C_i, \end{cases} \tag{22}$$

The Cauchy problem of the source terms (22) is an ordinary differential equation system that numerically can be approximated with an Euler step of length Δt,

$$\mathbf{u}_i^{n+1} = \mathbf{u}_i^{n+1,-} + \Delta t \cdot \mathbf{s}\big(\mathbf{u}_i^{n+1,-}\big). \tag{23}$$

For the discretization of the convective sub-system (21) the system is transformed in integral form by spatial integration over cell C_i and temporal integration from t^n to t^{n+1}. The spatial integral over the state vector is

[10] The construction of a symmetric positive definite matrix to show the symmetrizable property of the system matrix was also shown in [18], Part II, Section 2.5.2 for the primitive system vector $\tilde{\mathbf{u}} := \left(\alpha_1, \rho_2, v_2, p_2, \rho_1, v_1, p_1\right)^{\mathsf{T}}$.

approximated by its cell value,

$$\mathbf{u}_i^{n+1,-} = \mathbf{u}_i^n - \frac{\Delta t}{\Delta x}\left(\frac{1}{\Delta t}\int_{t^{n+1,-}}^{t^{n+1}}\int_{C_i} A(\mathbf{u})\,\partial_x \mathbf{u}\;\mathrm{d}x\;\mathrm{d}t\right). \tag{24}$$

Because the integrand of a non-conservative term is not defined for discontinuous functions $\mathbf{u}$, the term is expected to produce a Dirac measure [25]. To define weak solutions of this integral equation we need to approximate the non-conservative term. The general idea is to decompose the total mass of this Dirac measure into two summands $\mathbf{D}^{\pm}_{i+1/2}$. Thus, with an explicit Euler step in time and an approximation of the time integral of the non-conservative matrix, the update formulation of the finite volume method is given in *fluctuation* form [26, 27],

$$\mathbf{u}_i^{n+1,-} \;=\; \mathbf{u}_i^n - \frac{\Delta t}{\Delta x}\left(\mathbf{D}^-_{i+1/2} + \mathbf{D}^+_{i-1/2}\right). \tag{25}$$

To define weak solutions for the integral equation of the non-conservative system we follow Dal Maso, LeFloch and Murat [28], who proposed the path-conservative method, where the non-conservative term is interpreted as Borel measures over a Lipschitz continuous path $\Phi : [0,1]\times\Omega\times\Omega\to\Omega$ with

$$\Phi(0;\mathbf{u}_\mathrm{L},\mathbf{u}_\mathrm{R}) = \mathbf{u}_\mathrm{L},\;\; \Phi(1;\mathbf{u}_\mathrm{L},\mathbf{u}_\mathrm{R}) = \mathbf{u}_\mathrm{R},\;\; \Phi(s;\mathbf{u},\mathbf{u}) = \mathbf{u},\;\; \forall\,\mathbf{u}_\mathrm{L},\mathbf{u}_\mathrm{R},\mathbf{u}\in\Omega. \tag{26}$$

The path connects two states $\mathbf{u}_\mathrm{L}$ and $\mathbf{u}_\mathrm{R}$ at its left and right limits across a discontinuity with $s\in[0,1]$. Hence, the non-conservative matrix $A(\mathbf{u})$ is interpreted as $A(\Phi(s;\mathbf{u}_\mathrm{L},\mathbf{u}_\mathrm{R}))$. The chosen path of a weak solution influences the speed of propagation σ_Φ of the discontinuity. Thus, with the condition of *path consistency* [26], the generalized Rankine-Hugoniot condition [27, 29] holds,

$$\begin{aligned}\sigma_\Phi\cdot(\mathbf{u}_\mathrm{R}-\mathbf{u}_\mathrm{L}) &\overset{!}{=} \int_{\mathbf{u}_\mathrm{L}}^{\mathbf{u}_\mathrm{R}} A(\mathbf{u})\,\mathrm{d}\mathbf{u}\\ &= \mathbf{f}(\mathbf{u}_\mathrm{R})-\mathbf{f}(\mathbf{u}_\mathrm{L}) + \int_{\mathbf{u}_\mathrm{L}}^{\mathbf{u}_\mathrm{R}} B(\mathbf{u})\,\mathrm{d}\mathbf{u}\\ &= \mathbf{f}(\mathbf{u}_\mathrm{R})-\mathbf{f}(\mathbf{u}_\mathrm{L}) + \int_0^1 B\big(\Phi(s;\mathbf{u}_\mathrm{L},\mathbf{u}_\mathrm{R})\big)\frac{\partial\Phi(s;\mathbf{u}_\mathrm{L},\mathbf{u}_\mathrm{R})}{\partial s}\,\mathrm{d}s.\end{aligned} \tag{27}$$

The weak solutions now depend on the arbitrary chosen path Φ, where different families of paths lead to different jump conditions [27]. As already suggested in (25), the general idea is to decompose the total mass of this Dirac measure (27),

$$\mathbf{D}^-(\mathbf{u}_\mathrm{L},\mathbf{u}_\mathrm{R}) + \mathbf{D}^+(\mathbf{u}_\mathrm{L},\mathbf{u}_\mathrm{R}) \overset{!}{=} \mathbf{f}(\mathbf{u}_\mathrm{R})-\mathbf{f}(\mathbf{u}_\mathrm{L}) + \int_0^1 B\big(\Phi(s;\mathbf{u}_\mathrm{L},\mathbf{u}_\mathrm{R})\big)\frac{\partial\Phi(s;\mathbf{u}_\mathrm{L},\mathbf{u}_\mathrm{R})}{\partial s}\,\mathrm{d}s, \tag{28}$$

where the two *fluctuations* are Lipschitz continuous functions $\mathbf{D}^\pm:\Omega\times\Omega\to\Omega$. If furthermore it holds, that

$$\mathbf{D}^\pm(\mathbf{u},\mathbf{u}) = 0 \quad \forall\,\mathbf{u}\in\Omega, \tag{29}$$

the numerical scheme is said to be *path-consistent* [26]. By choosing a segment path, $\Phi(s;\mathbf{u}_\mathrm{L},\mathbf{u}_\mathrm{R}) := \mathbf{u}_\mathrm{L}+s\cdot(\mathbf{u}_\mathrm{R}-\mathbf{u}_\mathrm{L})$, the generalized Rankine-Hugoniot condition (27) simplifies to

$$\sigma_\Phi\cdot(\mathbf{u}_\mathrm{R}-\mathbf{u}_\mathrm{L}) \overset{!}{=} \mathbf{f}(\mathbf{u}_\mathrm{R})-\mathbf{f}(\mathbf{u}_\mathrm{L}) + \underbrace{\int_0^1 B\big(\Phi(s;\mathbf{u}_\mathrm{L},\mathbf{u}_\mathrm{R})\big)\,\mathrm{d}s}_{=:B_\Phi(\mathbf{u}_\mathrm{L},\mathbf{u}_\mathrm{R})}\;(\mathbf{u}_\mathrm{R}-\mathbf{u}_\mathrm{L}). \tag{30}$$

The matrix $B_\Phi(\mathbf{u}_\mathrm{L}, \mathbf{u}_\mathrm{R})$ is a local linearization of the system matrix $B(\mathbf{u})$ and is called *Roe matrix*, which can be approximated simply by the trapezoidal rule or by high-order Gaussian quadrature rules [30]. The integral form of a partial differential equation system forms the basis for the mathematical theory of weak solutions, including the derivation of the Rankine-Hugoniot conditions that govern the form and speed of shock waves [31]. But as non-conservative systems consist of parts which are based on differential equations, the Lax-Wendroff theorem for *mass conservation* is not guaranteed anymore [24].

Abgrall and Karni [29] and Castro et al. [27, 32] observed that the numerical solution of a path-conservative scheme with a suitable consistent selected path along the viscous profile, will not necessarily converge to the correct and physically relevant solution. This lack of convergence has its origin in the numerical viscosity of the scheme. Thus, we follow Tadmor who proposes to use the concept of *entropy-conservative* schemes [23].

For a given entropy pair (η, ψ) with entropy variables $\mathbf{v}(\mathbf{u}) := \partial_\mathbf{u}\eta(\mathbf{u})$, a path-consistent scheme (27) is said to be *entropy-conservative* [27] if the fluctuations are satisfying

$$\begin{aligned}\mathbf{v}_\mathrm{L}^\mathsf{T}\,\mathbf{D}_\mathrm{EC}^-(\mathbf{u}_\mathrm{L}, \mathbf{u}_\mathrm{R}) + \mathbf{v}_\mathrm{R}^\mathsf{T}\,\mathbf{D}_\mathrm{EC}^+(\mathbf{u}_\mathrm{L}, \mathbf{u}_\mathrm{R}) &\overset{!}{=} \int_0^1 \mathbf{v}\big(\Phi(s)\big)^\mathsf{T}\, A\big(\Phi(s)\big)\; \Phi'(s)\,\mathrm{d}s \\ &= \psi(\mathbf{u}_\mathrm{R}) - \psi(\mathbf{u}_\mathrm{L}).\end{aligned} \tag{31}$$

For a given family of paths, Castro et al. [27] show the existence of infinitely many entropy-conservative path-consistent schemes.[27]. With the artificial intermediate entropy variables $\mathbf{v}_\zeta := \mathbf{v}_\mathrm{L} + \zeta \cdot (\mathbf{v}_\mathrm{R} - \mathbf{v}_\mathrm{L})$ for $\zeta \in [0, 1]$ the fluctuations are given by

$$\mathbf{D}_\mathrm{EC}^\pm(\mathbf{u}_\mathrm{L}, \mathbf{u}_\mathrm{R}) = \int_0^1 V^\pm\big(\Phi(s)\big)^\mathsf{T}\; A\big(\Phi(s)\big)\; \Phi'(s)\,\mathrm{d}s, \tag{32}$$

while the matrices $V^\pm$ are chosen such that by construction it holds $V^- + V^+ = \mathcal{I}$ and $V^-\mathbf{v}_\mathrm{L} + V^+\mathbf{v}_\mathrm{R} = \mathbf{v}(\Phi)$,

$$V^\pm\big(\Phi(s)\big)^\mathsf{T} = \Big(\tfrac{1}{2} \pm (\zeta - \tfrac{1}{2})\Big)\,\mathcal{I} \pm \frac{\mathbf{v}_\mathrm{R} - \mathbf{v}_\mathrm{L}}{|\mathbf{v}_\mathrm{R} - \mathbf{v}_\mathrm{L}|^2}\,\Big(\mathbf{v}\big(\Phi(s)\big) - \mathbf{v}_\zeta\Big)^\mathsf{T}. \tag{33}$$

The integral can be approximated simply by the trapezoidal rule or by high-order Gaussian quadrature rules. Choosing $\zeta = \frac{1}{2}$ we get the *entropy-conservative Rusanov* scheme. With the above postulated condition of an entropy identity, it is ensured that entropy is never dissipated (what we just expect for smooth solutions). But for the case of shocks, we would assume that entropy is dissipated. Castro et al. [27] propose to consider the regularized equation, where numerical diffusion is added on the right-hand side,

$$\partial_t\mathbf{u} + \partial_x\mathbf{f}(\mathbf{u}) + B(\mathbf{u})\,\partial_x\mathbf{u} = \varepsilon_\mathrm{R}\,\partial_x\big(\mathcal{R}(\mathbf{u})\,\partial_x\mathbf{u}\big). \tag{34}$$

The viscosity matrix $\mathcal{R}(\mathbf{u})$ and its viscosity coefficient $\varepsilon_\mathrm{R} > 0$ are responsible for the observed lack of convergence to the physically relevant solutions in the ECPC scheme. This motivation turns into a new property for the scheme. A *path-consistent* scheme with *entropy-conservative* fluctuations $\mathbf{D}_\mathrm{EC}^\pm$ is said to be *entropy-stable* if its fluctuations are satisfying the following condition:

$$\mathbf{D}^\pm(\mathbf{u}_\mathrm{L}, \mathbf{u}_\mathrm{R}) = \mathbf{D}_\mathrm{EC}^\pm(\mathbf{u}_\mathrm{L}, \mathbf{u}_\mathrm{R}) \pm \frac{\varepsilon_\mathrm{R}}{\Delta x}\widehat{\mathcal{R}}(\mathbf{u}_\mathrm{L}, \mathbf{u}_\mathrm{R})\,(\mathbf{v}_\mathrm{R} - \mathbf{v}_\mathrm{L}). \tag{35}$$

For entropy stability, the numerical viscosity operator $\widehat{\mathcal{R}}(\mathbf{u}_\mathrm{L}, \mathbf{u}_\mathrm{R})$ must be a positive definite matrix. Therefore, we choose

$$\widehat{\mathcal{R}}(\mathbf{u}_\mathrm{L}, \mathbf{u}_\mathrm{R}) = \mathcal{R}(\mathbf{u}_\mathrm{L}, \mathbf{u}_\mathrm{R})\,\mathbf{u}'(\mathbf{v}). \tag{36}$$

with $\mathcal{R}$ as the viscosity matrix of the regularized equation (34). To obtain convergence to a correct solution it is essential to choose a suitable numerical diffusion operator that matches the underlying physical viscosity [33]. *Uniform viscosity* is given by $\mathcal{R} = \mathcal{I}$. The *Navier-Stokes viscosity* is not used, as it violates the minimum entropy principle if the thermal diffusivity is nonzero[11]. By choosing the numerical viscosity coefficient as

$$\varepsilon_{\mathrm{R}} = \frac{|\lambda_{\max}|}{2}\Delta x, \tag{37}$$

the term ε_{R} vanishes in the CFL condition [33], such that $\frac{\Delta t}{\Delta x} \cdot |\lambda_{\max}| \overset{!}{\leq} 0.5$.

4. Path-conservative approximate Godunov-Suliciu scheme

The entropy-preserving path-conservative finite volume methods have been developed to find the physically relevant solution, where the jump conditions are consistent with the viscous profiles. Another option is to develop a path-conservative version of the *Godunov* method, where the discrete cell averages are reconstructed by a simple piece-wise constant function. We denote $\mathbf{u}_{\mathrm{r}}^0 := \mathbf{u}_{\mathrm{r}}(0; \mathbf{u}_{\mathrm{L}}, \mathbf{u}_{\mathrm{R}})$ as the exact solution of the Riemann problem, which is known to be constant in time along the interface between two states $\mathbf{u}_{\mathrm{L}}$ and $\mathbf{u}_{\mathrm{R}}$. According to the definition of path-consistent schemes (28), the fluctuations for the Godunov scheme are given by [25]

$$\begin{aligned}
\mathbf{D}^-(\mathbf{u}_{\mathrm{L}}, \mathbf{u}_{\mathrm{R}}) &= \mathbf{f}\big(\mathbf{u}_{\mathrm{r}}^0\big) - \mathbf{f}\big(\mathbf{u}_{\mathrm{L}}\big) + B_\Phi(\mathbf{u}_{\mathrm{L}}, \mathbf{u}_{\mathrm{r}}^0)\,\big(\mathbf{u}_{\mathrm{r}}^0 - \mathbf{u}_{\mathrm{L}}\big),\\
\mathbf{D}^+(\mathbf{u}_{\mathrm{L}}, \mathbf{u}_{\mathrm{R}}) &= \mathbf{f}\big(\mathbf{u}_{\mathrm{R}}\big) - \mathbf{f}\big(\mathbf{u}_{\mathrm{r}}^0\big) + B_\Phi(\mathbf{u}_{\mathrm{r}}^0, \mathbf{u}_{\mathrm{R}})\,\big(\mathbf{u}_{\mathrm{R}} - \mathbf{u}_{\mathrm{r}}^0\big).
\end{aligned} \tag{38}$$

It remains to find the Riemann solution $\mathbf{u}_{\mathrm{r}}^0$. Because the pressure is non-linear, the conventional model provides genuinely nonlinear waves, such that the exact Riemann invariants cannot be found. We follow the relaxation approach of Suliciu [35, 36] and adapt it to the two-phase flow problem. Thus, we extend the original system with an additional balance law. Therefore, Suliciu intoduced the relaxation pressure π as a new parameter, which is defined by a Chapman-Enskog expansion of first order, $\pi := p + \varepsilon\pi^{(1)}$, such that for the relaxation time $\varepsilon \to 0$ it holds $\pi \to p$. The balance law of the relaxation pressure is given by

$$\partial_t(\alpha\rho\pi) + \partial_x(\alpha\rho v\pi) = -\underbrace{\alpha\rho^2 c^2}_{\approx a^2}\,\partial_x v + \alpha\rho\,\underbrace{\tfrac{1}{\varepsilon}(p-\pi)}_{=-\pi^{(1)}}. \tag{39}$$

The pre-factor of the velocity derivative, $\alpha\rho^2c^2$ is replaced by a constant parameter a^2, which is defined in (42). The *two-phase flow model* is extended by appending the relaxation pressure balance laws (39) for each phase. Additionally, all pressure terms p in the mass, momentum and energy balance laws are replaced by π, such that a *relaxation two-phase flow model* with nine equations[12] is reached,

$$\partial_t\tilde{\mathbf{u}} + \partial_x\tilde{\mathbf{f}}(\tilde{\mathbf{u}}) + \tilde{B}(\tilde{\mathbf{u}})\,\partial_x\tilde{\mathbf{u}} = \mathbf{s}_{\mathrm{r}}(\tilde{\mathbf{u}}) + \tilde{\mathbf{s}}(\tilde{\mathbf{u}}), \tag{40}$$

with $\tilde{\mathbf{u}} = \big(\alpha_1,\, \alpha_1\rho_1,\, \alpha_1\rho_1 v_1,\, \alpha_1\rho_1 E_1,\, \alpha_1\rho_1\pi_1,\, \alpha_2\rho_2,\, \alpha_2\rho_2 v_2,\, \alpha_2\rho_2 E_2,\, \alpha_2\rho_2\pi_2\big)^{\mathsf{T}}$. For the closed quasilinear form we define $\tilde{A}(\tilde{\mathbf{u}}) := \partial_{\tilde{\mathbf{u}}}\tilde{\mathbf{f}}(\tilde{\mathbf{u}}) + \tilde{B}(\tilde{\mathbf{u}})$. In the following we will see that by construction, the enlarged model has the same thermodynamical and mathematical properties as the original system.

[11] See Serre [34], Theorem 8.2.3

[12] The fully expanded parameters $\tilde{\mathbf{u}}$, $\tilde{\mathbf{f}}$, $\tilde{B}$, $\mathbf{s}_{\mathrm{r}}$, $\tilde{\mathbf{s}}$ and the corresponding system matrix $\tilde{A}$ can be found in [18], Part II, Eq. (5.49)ff.

4.1. Properties of the relaxation two-phase flow model

The system admits nine real eigenvalues which are all real but not necessarily distinct,

$$\tilde{\lambda}_1 = v_1 - \frac{a_1}{\rho_1\sqrt{\alpha_1}},\ \tilde{\lambda}_2 = v_2 - \frac{a_2}{\rho_2\sqrt{\alpha_2}},\ \tilde{\lambda}_3 = v_1,\ \tilde{\lambda}_4 = v_\mathrm{i},\ \tilde{\lambda}_5 = v_2,\ \tilde{\lambda}_6 = v_1 + \frac{a_1}{\rho_1\sqrt{\alpha_1}},\ \tilde{\lambda}_7 = v_2 + \frac{a_2}{\rho_2\sqrt{\alpha_2}}, \quad (41)$$

where λ_3 and λ_5 are double eigenvalues. To fulfill the *sub-characteristic condition*[13], we choose

$$a_1 \geq \sqrt{\alpha_1}\rho_1 c_1 \quad \text{and} \quad a_2 \geq \sqrt{\alpha_2}\rho_2 c_2, \quad (42)$$

such that the wave velocities of the origin system never exceed the corresponding wave velocities in the extended system [37], see also Whitham [38] and Liu [39]. This choice furthermore fulfills the *non-resonance condition*, $v_\mathrm{i} \neq v_1 \pm \frac{a_1}{\rho_1\sqrt{\alpha_1}}$ and $v_\mathrm{i} \neq v_2 \pm \frac{a_2}{\rho_2\sqrt{\alpha_2}}$, such that the corresponding eigenvectors are linearly independent and therefore the system is *hyperbolic*[14]. As in Subsection 2.4 it can be shown that with the entropy-entropy flux pair (16) the relaxation model is consistent with the *second law of thermodynamics*[15]. In comparison to the original entropy variables in (18) we get the additional entries $-\frac{1}{T_1}$ and $-\frac{1}{T_2}$ for the relaxation pressure in $\tilde{\mathbf{v}}(\tilde{\mathbf{u}})$. Furthermore, as before it can be shown that the relaxed system is *symmetrizable*[16] [18].

4.2. Characteristic fields

The motivation to construct a relaxation model was to obtain a system, such that all *characteristic fields* of the relaxation model are linearly degenerate[17]. Thus, for each eigenvalue $\tilde{\lambda}_j$ and its corresponding right eigenvector R_j it should hold $\partial_{\tilde{\mathbf{u}}}\tilde{\lambda}_j\, R_j = 0$ [19]. Note that the eigenvalue v_i was already chosen in equation (9), such that its associated field is linearly degenerated. Each j-characteristic field has several j-Riemann invariants $\mathbf{w}_p^{(j)}$, which are constant along the trajectories of the vector field R_j:

$$\partial_{\tilde{\mathbf{u}}}\mathbf{w}_p^{(j)}\, R_j \stackrel{!}{=} 0, \quad (43)$$

[13] The *sub-characteristic condition* for the relaxed two-phase flow model was also shown in [18], Part II, Section 5.3.4.
[14] *Hyperbolicity* for the relaxed two-phase flow model was also shown in [18], Part II, Section 5.3.2.
[15] The *entropy inequality* for the relaxed two-phase flow model was also shown in [18], Part II, Section 5.3.1.
[16] The *symmetrization* of the relaxed two-phase flow model was also shown in [18], Part II, Section 5.3.5.
[17] The characteristic field of the relaxed two-phase flow model was shown in [18], Part II, Section 5.3.3

From this definition it is obvious to see that $\tilde{\lambda}_j$ is also a j-Riemann invariant if the j-characteristic field is linearly degenerated [24]. The j-Riemann invariants are given by [18]:

$$
\begin{aligned}
\mathbf{w}^{(1)} &= \left\{ \alpha_1, \rho_2, v_2, u_2, \pi_2, v_1 - \frac{a_1}{\rho_1\sqrt{\alpha_1}}, \pi_1 + v_1\frac{a_1}{\sqrt{\alpha_1}}, -\tfrac{1}{2}\pi_1^2 + u_1\frac{a_1^2}{\alpha_1} \right\}, \\
\mathbf{w}^{(2)} &= \left\{ \alpha_1, \rho_1, v_1, u_1, \pi_1, v_2 - \frac{a_2}{\rho_2\sqrt{\alpha_2}}, \pi_2 + v_2\frac{a_2}{\sqrt{\alpha_2}}, -\tfrac{1}{2}\pi_2^2 + u_2\frac{a_2^2}{\alpha_2} \right\}, \\
\mathbf{w}^{(3)} &= \Big\{ \alpha_1, v_1, \pi_1, \rho_2, v_2, u_2, \pi_2 \Big\}, \\
\mathbf{w}^{(4)} &= \Big\{ v_\mathrm{i},\ \ \alpha_2\rho_2(v_2 - v_\mathrm{i}),\ \ u_1 + \frac{\pi_1}{\rho_1} + \tfrac{1}{2}(v_1 - v_\mathrm{i})^2,\ \ u_2 + \frac{\pi_2}{\rho_2} + \tfrac{1}{2}(v_2 - v_\mathrm{i})^2, \\
&\qquad \alpha_1\rho_1\pi_1(v_1 - v_\mathrm{i}) + a_1^2 v_1,\ \ \alpha_2\rho_2\pi_2(v_2 - v_\mathrm{i}) + a_2^2 v_2, \\
&\qquad \alpha_1\rho_1 s_1(v_1 - v_\mathrm{i}) + \alpha_2\rho_2 s_2(v_2 - v_\mathrm{i}),\ \ \alpha_1\big(\pi_1 + \rho_1 v_1(v_1 - v_\mathrm{i})\big) + \alpha_2\big(\pi_2 + \rho_2 v_2(v_2 - v_\mathrm{i})\big) \Big\}, \\
\mathbf{w}^{(5)} &= \Big\{ \alpha_1, \rho_1, v_1, u_1, \pi_1, v_2, \pi_2 \Big\}, \\
\mathbf{w}^{(6)} &= \left\{ \alpha_1, \rho_2, v_2, u_2, \pi_2, v_1 + \frac{a_1}{\rho_1\sqrt{\alpha_1}}, \pi_1 - v_1\frac{a_1}{\sqrt{\alpha_1}}, -\tfrac{1}{2}\pi_1^2 + u_1\frac{a_1^2}{\alpha_1} \right\}, \\
\mathbf{w}^{(7)} &= \left\{ \alpha_1, \rho_1, v_1, u_1, \pi_1, v_2 + \frac{a_2}{\rho_2\sqrt{\alpha_2}}, \pi_2 - v_2\frac{a_2}{\sqrt{\alpha_2}}, -\tfrac{1}{2}\pi_2^2 + u_2\frac{a_2^2}{\alpha_2} \right\}.
\end{aligned}
\tag{44}
$$

Due to the non-linearities of the v_i-Riemann invariants, the intermediate states of the Riemann problem are difficult to determine. An approximate solution can be obtained by weaken the nonlinear Rankine-Hugoniot conditions at the v_i-contact discontinuity. Thus, we propose the following approximated v_i Riemann invariants:

$$
\mathbf{w}^{(4)}_{\mathrm{approx}} := \left\{ v_1, \pi_1, v_2, \pi_2, \alpha_1\rho_1, \alpha_2\rho_2, u_1 + \frac{\pi_1}{\rho_1}, u_2 + \frac{\pi_2}{\rho_2} \right\} \tag{45}
$$

As for the original v_i-Riemann invariants $\mathbf{w}^{(4)}$ it holds that for the case of equal volume fractions $\alpha_\mathrm{L} = \alpha_\mathrm{R}$ at the left-hand and right-hand side of the Riemann problem, the spatial derivative of the volume fraction is zero, such that the Riemann invariants of the v_i-wave reduce to $\mathbf{w}^{(4)}_{\alpha_\mathrm{L}=\alpha_\mathrm{R}} = \{\rho_1, v_1, u_1, \pi_1, \rho_2, v_2, u_2, \pi_2\}$. Furthermore, with this choice of $\mathbf{w}^{(4)}_{\mathrm{approx}}$ at least six out of eight original Rankine-Hugoniot conditions are always fulfilled. Just the fifth $\mathbf{w}^{(1)}_5$ and sixth $\mathbf{w}^{(1)}_6$ of the original v_i-Riemann invariant can be unfulfilled due to the hidden void fraction α in a_1 and a_2.

4.3. Riemann solver for the relaxation two-velocity two-pressure model

The v_i-contact discontinuity is the only wave which changes the volume fraction α_1 and thus enforces an exchange of the liquid and steam phase. The other six waves act like two independent Euler systems: they just affect their own phase without having influence on the other phase nor the volume fraction. To develop a Riemann solver we need to order the eigenvalues (41) and formulate an equation system from the Rankine-Hugoniot jump relations across the discontinuities.

For subsonic flow, it is clear that the eigenvalues which contain the speed of sound (hidden in the parameter a_1 and a_2) are the slowest $(\tilde{\lambda}_1, \tilde{\lambda}_2)$ and fastest $(\tilde{\lambda}_6, \tilde{\lambda}_7)$. Furthermore, as $\tilde{\lambda}_4 = v_\mathrm{i}$ was chosen as convex combination of $\tilde{\lambda}_3 = v_1$ and $\tilde{\lambda}_5 = v_2$, see (9), the interfacial velocity is ordered in-between the phasic velocities. This gives us the

following order of the eigenvalues:

$$\min\left\{\tilde{\lambda}_1,\tilde{\lambda}_2\right\} \;\leq\; \max\left\{\tilde{\lambda}_1,\tilde{\lambda}_2\right\} \;<\; \min\left\{\tilde{\lambda}_3,\tilde{\lambda}_5\right\} \;\leq\; \tilde{\lambda}_4 \;\leq\; \max\left\{\tilde{\lambda}_3,\tilde{\lambda}_5\right\} \;<\; \min\left\{\tilde{\lambda}_6,\tilde{\lambda}_7\right\} \;\leq\; \max\left\{\tilde{\lambda}_6,\tilde{\lambda}_7\right\}. \tag{46}$$

A contact discontinuity with corresponding characteristic speed $\tilde{\lambda}_j$ separates two neighboring states $\tilde{\mathbf{u}}_{j-1}$ and $\tilde{\mathbf{u}}_j$, see Figure 1. As the corresponding j-Riemann invariants $\mathbf{w}^{(j)}$ are constant across the contact discontinuities it must hold $\mathbf{w}^{(j)}(\tilde{\mathbf{u}}_{j-1}) \overset{!}{=} \mathbf{w}^{(j)}(\tilde{\mathbf{u}}_j)$.

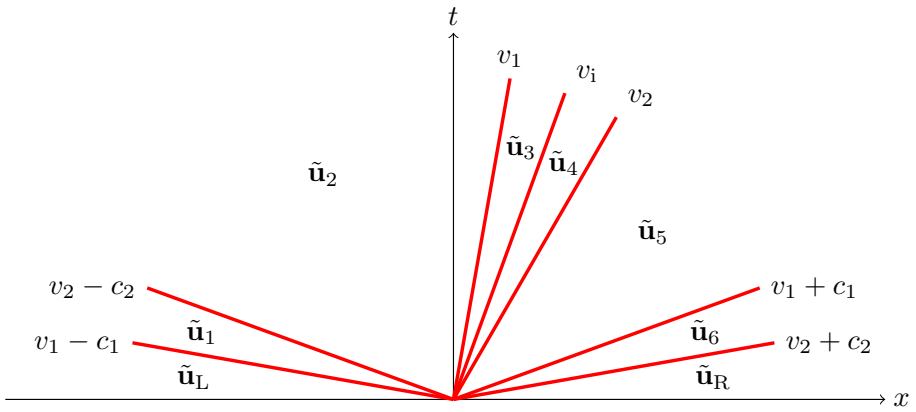

Figure 1: Sketch of the solution of the Riemann problem with ordered eigenvalues and given left $\tilde{\mathbf{u}}_\mathrm{L}$ and right $\tilde{\mathbf{u}}_\mathrm{R}$ state. The Rankine-Hugoniot jump relations across the discontinuities are used to find the six intermediate states $\tilde{\mathbf{u}}_j$.

For the Godunov solver the solution at the interface position $x = 0$ between two states $\tilde{\mathbf{u}}_\mathrm{L}$ and $\tilde{\mathbf{u}}_\mathrm{R}$ is needed. Thus, for subsonic flow we are mainly interested in the intermediate states $\tilde{\mathbf{u}}_2$ to $\tilde{\mathbf{u}}_5$. As the neighboring contact discontinuities $\tilde{\lambda}_1$ and $\tilde{\lambda}_2$ affect different phases, the solution of the intermediate state $\tilde{\mathbf{u}}_2$ does not depend on the order of these waves in (46). The same holds for the contact discontinuities $\tilde{\lambda}_6$ and $\tilde{\lambda}_7$ with the intermediate state $\tilde{\mathbf{u}}_5$. Now using the Rankine-Hugoniot jump relations across the discontinuities we obtain the following primitive parameters of the unknown intermediate states in dependency of the known left $\mathbf{u}_\mathrm{L}$ and right state $\mathbf{u}_\mathrm{R}$:

$$\tilde{\mathbf{u}}_2^{\mathrm{prim}} = \begin{pmatrix} (\alpha)_\mathrm{L} \\ (\rho_1)_2 \\ (v_1)_\star \\ (u_1)_2 \\ (\pi_1)_\star \\ (\rho_2)_2 \\ (v_2)_\star \\ (u_2)_2 \\ (\pi_2)_\star \end{pmatrix}, \quad \tilde{\mathbf{u}}_3^{\mathrm{prim}} = \begin{pmatrix} (\alpha)_\mathrm{L} \\ (\rho_1)_3 \\ (v_1)_\star \\ (u_1)_3 \\ (\pi_1)_\star \\ (\rho_2)_3 \\ (v_2)_\star \\ (u_2)_3 \\ (\pi_2)_\star \end{pmatrix}, \quad \tilde{\mathbf{u}}_4^{\mathrm{prim}} = \begin{pmatrix} (\alpha)_\mathrm{R} \\ (\rho_1)_4 \\ (v_1)_\star \\ (u_1)_4 \\ (\pi_1)_\star \\ (\rho_2)_4 \\ (v_2)_\star \\ (u_2)_4 \\ (\pi_2)_\star \end{pmatrix}, \quad \tilde{\mathbf{u}}_5^{\mathrm{prim}} = \begin{pmatrix} (\alpha)_\mathrm{R} \\ (\rho_1)_5 \\ (v_1)_\star \\ (u_1)_5 \\ (\pi_1)_\star \\ (\rho_2)_5 \\ (v_2)_\star \\ (u_2)_5 \\ (\pi_2)_\star \end{pmatrix}. \tag{47}$$

To ensure that the order of the contact waves also holds for the determined intermediate states we choose $(a_k)_*$ large enough (for the phases $k = 1, 2$) with

$$(a_k)_* > \max\left\{ (a_k)_\mathrm{L}, \; (a_k)_\mathrm{R} \right\}. \tag{48}$$

Furthermore, we get from the Rankine-Hugoniot conditions the velocity

$$(v_k)_\star = \frac{(v_k)_{\mathrm{R}}\sqrt{(\alpha_k)_{\mathrm{L}}}+(v_k)_{\mathrm{L}}\sqrt{(\alpha_k)_{\mathrm{R}}}}{\sqrt{(\alpha_k)_{\mathrm{L}}}+\sqrt{(\alpha_k)_{\mathrm{R}}}} + \frac{\sqrt{(\alpha_k)_{\mathrm{L}}}\sqrt{(\alpha_k)_{\mathrm{R}}}\big((\pi_k)_{\mathrm{L}}-(\pi_k)_{\mathrm{R}}\big)}{(a_k)_*\left(\sqrt{(\alpha_k)_{\mathrm{L}}}+\sqrt{(\alpha_k)_{\mathrm{R}}}\right)}, \tag{49}$$

the relaxed pressure

$$(\pi_k)_\star = \frac{(a_k)_*(v_k)_{\mathrm{L}}-(a_k)_*(v_k)_{\mathrm{R}}+(\pi_k)_{\mathrm{L}}\sqrt{(\alpha_k)_{\mathrm{L}}}+(\pi_k)_{\mathrm{R}}\sqrt{(\alpha_k)_{\mathrm{R}}}}{\sqrt{(\alpha_k)_{\mathrm{L}}}+\sqrt{(\alpha_k)_{\mathrm{R}}}}, \tag{50}$$

the density

$$\begin{aligned}
(\rho_k)_2 &= \left(\frac{1}{(\rho_k)_{\mathrm{L}}} + \Big((v_k)_\star - (v_k)_{\mathrm{L}}\Big)\frac{\sqrt{(\alpha_k)_{\mathrm{L}}}}{(a_k)_*}\right)^{-1},\\
(\rho_1)_3 &= \begin{cases} (\rho_1)_2 & , \text{ if } (v_1)_\star > (v_2)_\star \\ (\rho_1)_5\,\frac{(\alpha_1)_{\mathrm{R}}}{(\alpha_1)_{\mathrm{L}}} & , \text{ else} \end{cases}\\
(\rho_2)_3 &= \begin{cases} (\rho_2)_5\,\frac{(\alpha_2)_{\mathrm{R}}}{(\alpha_2)_{\mathrm{L}}} & , \text{ if } (v_1)_\star > (v_2)_\star \\ (\rho_2)_2 & , \text{ else} \end{cases}\\
(\rho_1)_4 &= \begin{cases} (\rho_1)_2\,\frac{(\alpha_1)_{\mathrm{L}}}{(\alpha_1)_{\mathrm{R}}} & , \text{ if } (v_1)_\star > (v_2)_\star \\ (\rho_1)_5 & , \text{ else} \end{cases}\\
(\rho_2)_4 &= \begin{cases} (\rho_2)_5 & , \text{ if } (v_1)_\star > (v_2)_\star \\ (\rho_2)_2\,\frac{(\alpha_2)_{\mathrm{L}}}{(\alpha_2)_{\mathrm{R}}} & , \text{ else} \end{cases}\\
(\rho_k)_5 &= \left(\frac{1}{(\rho_k)_{\mathrm{R}}} - \Big((v_k)_\star - (v_k)_{\mathrm{R}}\Big)\frac{\sqrt{(\alpha_k)_{\mathrm{R}}}}{(a_k)_*}\right)^{-1},
\end{aligned} \tag{51}$$

and the specific inner energy

$$\begin{aligned}
(u_k)_2 &= (u_k)_{\mathrm{L}} + \Big((\pi_k)_\star^2 - (\pi_k)_{\mathrm{L}}^2\Big)\frac{(\alpha_k)_{\mathrm{L}}}{2(a_k)_*^2},\\
(u_1)_3 &= \begin{cases} (u_1)_2 & , \text{ if } (v_1)_\star > (v_2)_\star \\ (u_1)_5 + \frac{(\alpha_1)_{\mathrm{R}}-(\alpha_1)_{\mathrm{L}}}{(\alpha_1)_{\mathrm{R}}}\cdot\frac{(\pi_1)_\star}{(\rho_1)_5} & , \text{ else} \end{cases}\\
(u_2)_3 &= \begin{cases} (u_2)_5 + \frac{(\alpha_2)_{\mathrm{R}}-(\alpha_2)_{\mathrm{L}}}{(\alpha_2)_{\mathrm{R}}}\cdot\frac{(\pi_2)_\star}{(\rho_2)_5} & , \text{ if } (v_1)_\star > (v_2)_\star \\ (u_2)_2 & , \text{ else} \end{cases}\\
(u_1)_4 &= \begin{cases} (u_1)_2 + \frac{(\alpha_1)_{\mathrm{L}}-(\alpha_1)_{\mathrm{R}}}{(\alpha_1)_{\mathrm{L}}}\cdot\frac{(\pi_1)_\star}{(\rho_1)_2} & , \text{ if } (v_1)_\star > (v_2)_\star \\ (u_1)_5 & , \text{ else} \end{cases}\\
(u_2)_4 &= \begin{cases} (u_2)_5 & , \text{ if } (v_1)_\star > (v_2)_\star \\ (u_2)_2 + \frac{(\alpha_2)_{\mathrm{L}}-(\alpha_2)_{\mathrm{R}}}{(\alpha_2)_{\mathrm{L}}}\cdot\frac{(\pi_2)_\star}{(\rho_2)_2} & , \text{ else} \end{cases}\\
(u_k)_5 &= (u_k)_{\mathrm{R}} + \Big((\pi_k)_\star^2 - (\pi_k)_{\mathrm{R}}^2\Big)\frac{(\alpha_k)_{\mathrm{R}}}{2(a_k)_*^2}.
\end{aligned} \tag{52}$$

Now, we can develop the interfacial velocity at intermediate state $(v_{\mathrm{i}})_*$ from formula (11). As v_{i} is an eigenvalue, we can wither use the values from neighboring state at the left-hand side $\tilde{\mathbf{u}}_3$ or on the right-hand side $\tilde{\mathbf{u}}_4$,

$$(v_{\mathrm{i}})_* := \frac{(1-\xi)\,(\alpha_1)_{\mathrm{L}}\,(\rho_1)_3\,(v_1)_\star + \xi\,(\alpha_2)_{\mathrm{L}}\,(\rho_2)_3\,(v_2)_\star}{(1-\xi)\,(\alpha_1)_{\mathrm{L}}\,(\rho_1)_3 + \xi\,(\alpha_2)_{\mathrm{L}}\,(\rho_2)_3} = \frac{(1-\xi)\,(\alpha_1)_{\mathrm{R}}\,(\rho_1)_4\,(v_1)_\star + \xi\,(\alpha_2)_{\mathrm{R}}\,(\rho_2)_4\,(v_2)_\star}{(1-\xi)\,(\alpha_1)_{\mathrm{R}}\,(\rho_1)_4 + \xi\,(\alpha_2)_{\mathrm{R}}\,(\rho_2)_4}. \tag{53}$$

Altogether, the Riemann solution is now given by

$$\tilde{\mathbf{u}}_{\mathrm{r}}(0) = \begin{cases} \tilde{\mathbf{u}}_2 & , \text{ if } & & & 0 & < & \min\left((v_2)_\star, (v_1)_\star\right), \\ \tilde{\mathbf{u}}_3 & , \text{ if } & \min\left((v_2)_\star, (v_1)_\star\right) & < & 0 & < & (v_{\mathrm{i}})_\star, \\ \tilde{\mathbf{u}}_4 & , \text{ if } & (v_{\mathrm{i}})_\star & < & 0 & < & \max\left((v_2)_\star, (v_1)_\star\right), \\ \tilde{\mathbf{u}}_5 & , \text{ if } & \max\left((v_2)_\star, (v_1)_\star\right) & < & 0. & & \end{cases} \tag{54}$$

5. Case study

To investigate the behavior of the developed schemes, several test cases have been performed. For comparability of the results we use adaptive time steps with a CFL number of 0.45.

5.1. Isolated coupling wave

As a first test for the two-phase flow model, a problem of Gallouët, Hérard, and Seguin [16] is used, which produces a moving contact discontinuity. The interfacial modeling parameter (10) for this problem is given by $\xi = 0.5$. For the domain $x \in [0, 1000]$ a Riemann problem is defined at $x = 500$, where the initial values are given in Table 1. As closure, ideal gas with $\gamma_1 = \gamma_2 = 1.4$ and $c_{\mathrm{v}_1} = c_{\mathrm{v}_2} = 718$ J/kg K is chosen. The simulation time is $t_{\max} = 3$ sec.

	α_1	ρ_1	v_1	p_1	ρ_2	v_2	p_2
Left	0.9	1	100	10^5	1	100	10^5
Right	0.5	0.125	100	10^5	0.125	100	10^5

Table 1: Initial values for the *isolated coupling wave* problem.

Because all velocities are chosen equal, the volume fraction propagates with constant speed of 100 m/s, such that its exact solution is known, where the shock position of α moves from position $x = 500$ to $x = 800$.

In Figure 2 grid refinement results of the volume fraction α are shown, using the approximate Godunov-Suliciu (PC) solver and the Rusanov (ESPC) solver. It can be seen that both schemes converge to the exact solution, while the convergence of the Godunov-Suliciu (PC) is faster than the Rusanov (ESPC) scheme.

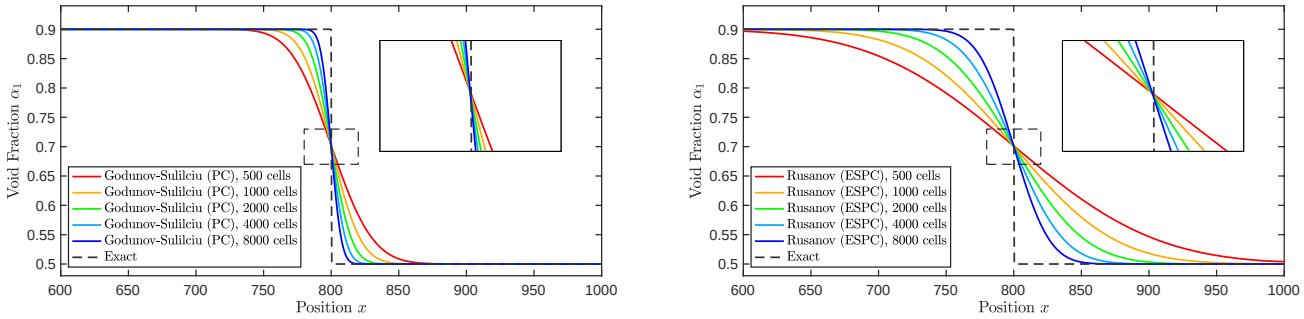

Figure 2: Grid refinement for the *isolated coupling wave* problem at $t_{\max} = 3$. The results for the volume fraction α_1 are shown (zoomed around the shock position), using the (left) Godunov Suliciu (PC) scheme, and the (right) Rusanov (ESPC) scheme.

As the exact solution of the volume fraction α_1 is known, this parameter is used as a measure for the accuracy in the L_1, L_2 and L_∞ norm, see Table 2. In Figure 3 (a), the L_2-error is plotted against the number of grid cells.

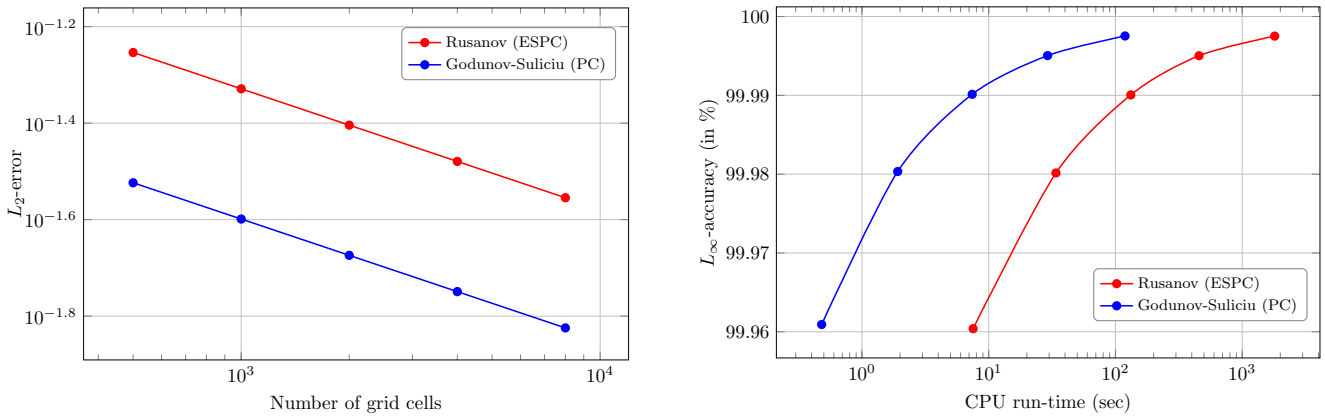

(a) Convergence of accuracy

(b) Run-time analysis

Figure 3: L_2-error against the number of grid cells (a) and run-time analysis (b) for the Rusanov (ESPC) and Godunov-Suliciu (PC) scheme. The accuracy of the run-time analysis is measured in the L_∞ error norm.

It can be seen that the empirical order of convergence is the same for both schemes, whereas the entropy-stable scheme is more dissipative. The accuracy of the different schemes related to the CPU run-time[18] is depicted in Figure 3 (b). The reason for the larger run-times for the Rusanov (ESPC) scheme comes from the approximation of the integral along the path with a numerical quadrature rule in (32).

Number of grid cells	Rusanov (ESPC)			Godunov-Suliciu (PC)		
	L_1	L_2	L_∞	L_1	L_2	L_∞
500	0.026474	0.055776	0.0003962	0.0076614	0.029954	0.0003908
1000	0.01878	0.046908	0.00019866	0.005419	0.025194	0.00019675
2000	0.0038323	0.021188	9.885e-05	0.013283	0.039448	9.9551e-05
4000	0.0093911	0.03317	4.9832e-05	0.00271	0.017818	4.9593e-05
8000	0.0066405	0.027892	2.4941e-05	0.0019164	0.014984	2.4856e-05

Table 2: Convergence analysis of the Rusanov (ESPC) and Godunov-Suliciu (PC) schemes using the L_1, L_2, and L_∞ norm to measure the error.

[18]The run-time highly depends on the implementation. For comparison reasons we measure the evaluation time in every grid cell for both fluxes without re-using information from the neighboring cell.

5.2. *Pressure disequilibrium*

The *pressure disequilibrium* test case [16] is a more difficult version of the isolated coupling wave. This test case was performed to investigate the Riemann invariants at the v_i-contact discontinuity. In comparison to the previous test case in 5.1 we only change the initial values according to Table 3 and the simulation time to $t_\mathrm{max} = 0.7$ sec [13]. As reference solution, the Godunov-Suliciu (PC) solver with 100 000 cells is used.

	α_1	ρ_1	v_1	p_1	ρ_2	v_2	p_2
Left	0.9	1	0	10^5	10	0	10^4
Right	0.5	0.125	0	10^4	1.25	0	10^3

Table 3: Initial values for the *pressure disequilibrium* problem.

In the following Figures 4 and 5 grid refinement results for the partial mass $\alpha_k\rho_k$ of both phases are shown, using the approximate Godunov-Suliciu (PC) solver and the Rusanov (ESPC) solver. It can be seen that both methods converge to the reference solution, while again the entropy-stable scheme converges slower than the relaxation scheme.

In Figure 6 the Riemann invariants at the v_i contact discontinuity defined in equations (44) are shown (just zoomed around the position of the corresponding wave). As expected for the approximate Godunov-Suliciu (PC) scheme, we see a smooth behavior of the Riemann invariants at the contact discontinuity (at $x \approx 605$). Furthermore, the fifth $\mathbf{w}_5^{(1)}$ and sixth $\mathbf{w}_6^{(1)}$ Riemann invariant show some "delayed corrections" (at $x \in [605, 615]$), which comes due to the simplification we made in (45). It is interesting to see that the entropy-stable Rusanov scheme has jumps in every Riemann invariant. It may be that the chosen uniform viscosity for (36) is not the best choice for this problem.

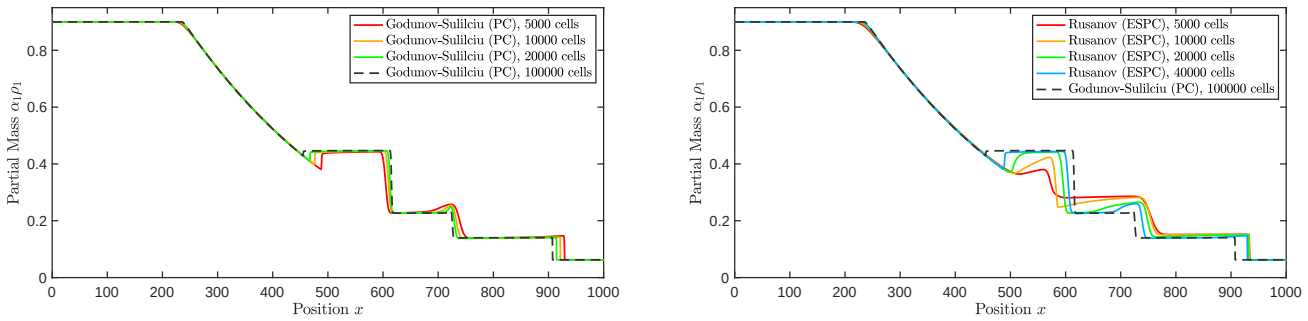

Figure 4: Grid refinement for the *pressure disequilibrium* problem at $t_\mathrm{max} = 0.7$. The results for the partial mass $\alpha_1\rho_1$ are shown, using the (left) Godunov Suliciu (PC) scheme, and the (right) Rusanov (ESPC) scheme.

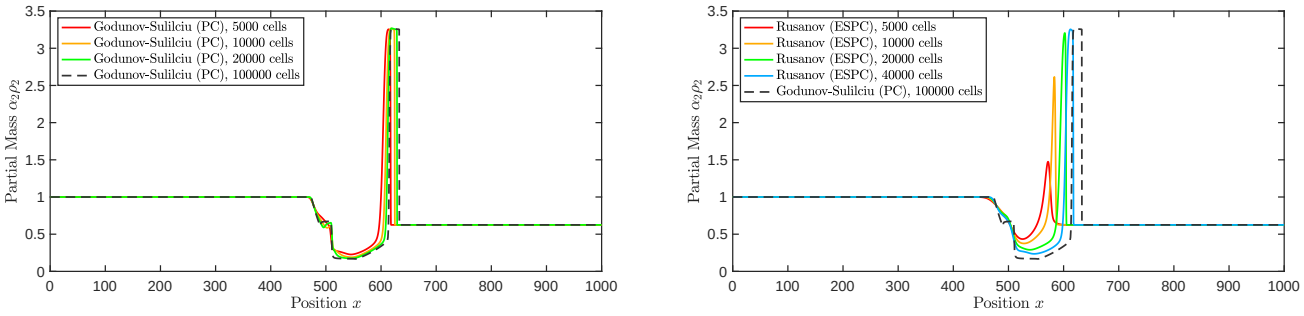

Figure 5: Grid refinement for the *pressure disequilibrium* problem at $t_{\max} = 0.7$. The results for the partial mass $\alpha_2\rho_2$ are shown, using the (left) Godunov Suliciu (PC) scheme, and the (right) Rusanov (ESPC) scheme.

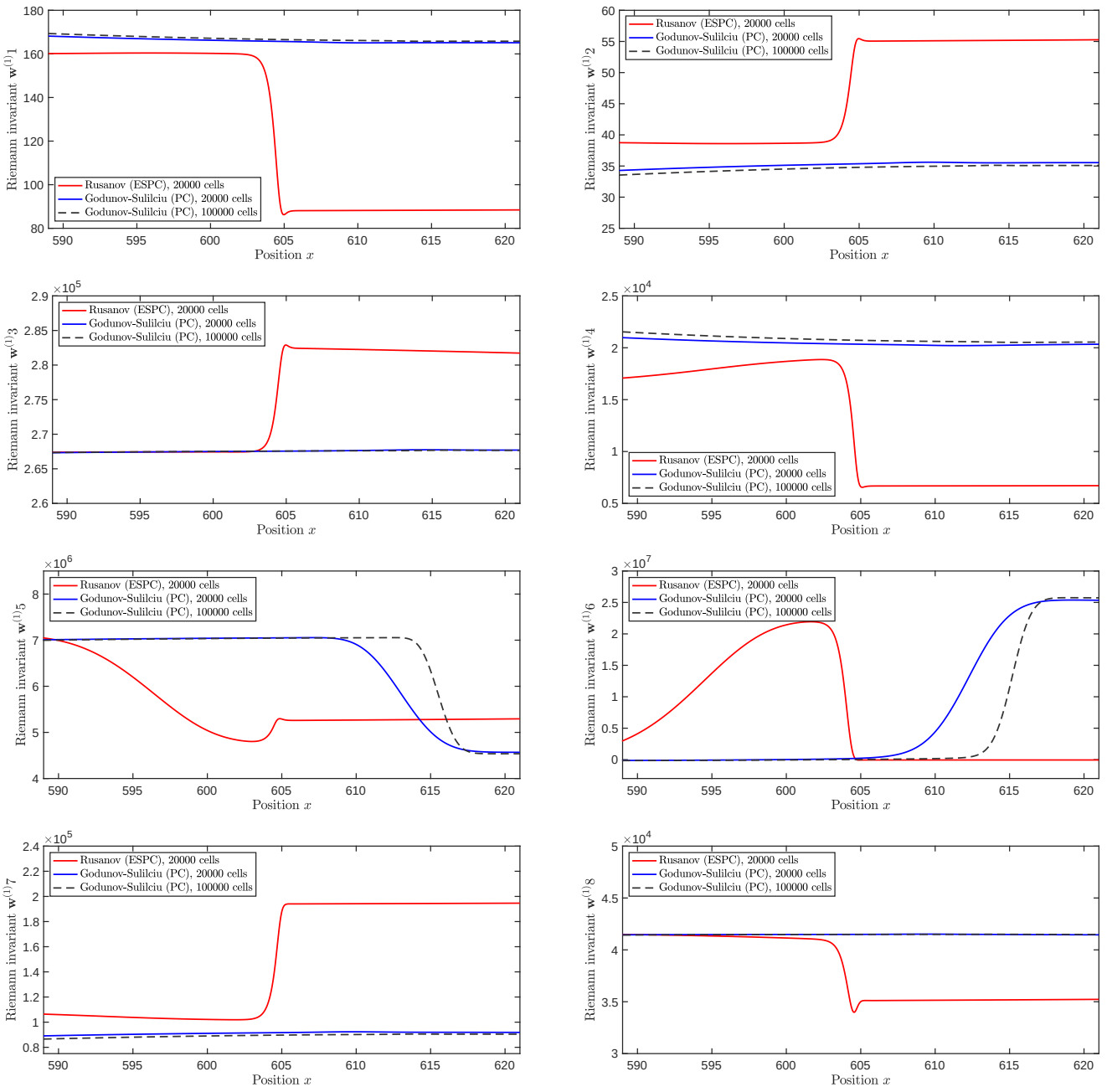

Figure 6: Riemann invariants at the v_{i}-contact discontinuity for the *pressure disequilibrium* problem at $t_{\max} = 0.7$ (just showing the region around the position of the corresponding wave at about $x = 605$).

5.3. Mixture at rest with increase in the volume fraction

This test case was proposed by Schwendeman, Wahle and Kapila [40] and is used to investigate the impact of the interfacial modeling parameter ξ, which defines the interfacial pressure p_{i} (20) and interfacial velocity v_{i} (11). For the domain $x \in [0, 1]$ a Riemann problem is defined at $x = 0.5$, where the initial values are given in Table 4. As closure, ideal gas with $\gamma_1 = \gamma_2 = 1.4$ and $c_{\mathrm{v}_1} = c_{\mathrm{v}_2} = 718$ J/kg K is chosen. The simulation time is $t_{\max} = 0.2$ sec.

	α_1	ρ_1	v_1	p_1	ρ_2	v_2	p_2
Left	0.8	1	0	1	0.2	0	0.3
Right	0.3	1	0	1	1	0	1

Table 4: Initial values for the *mixture at rest* problem.

In the following Figures 7 and 8 the phasic velocity v_1 and v_2 at different phasic mixtures $\xi \in [0, 1]$ are shown, using the approximate Godunov-Suliciu (PC) solver and the Rusanov (ESPC) solver. The results show a good agreements among both solvers. It can be seen that the solution strongly depends on the choice of the parameter ξ.

In Figure 9 the total entropy dissipation $\eta(t_n) := \Delta x \cdot \sum_{i=1}^{N} \eta(\mathbf{u}_i^n)$ for different meshes is plotted. It can be observed that the entropy dissipation for both solvers converge in different speeds in direction to the reference solution, what shows that both schemes satisfy the entropy inequality (14).

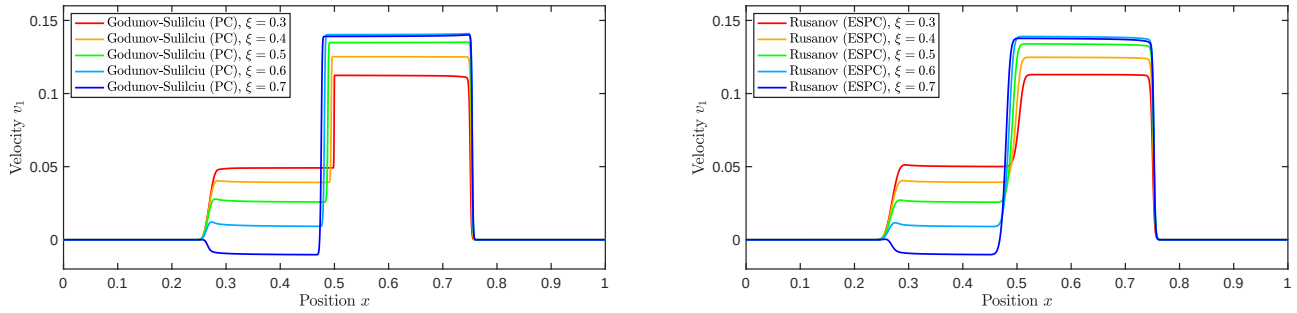

Figure 7: Different phasic mixtures ξ for the *mixture at rest* problem at $t_{\max} = 0.2$ using 16 000 cells. The results for the phasic velocity v_1 are shown, using the (left) Godunov Suliciu (PC) scheme, and the (right) Rusanov (ESPC) scheme.

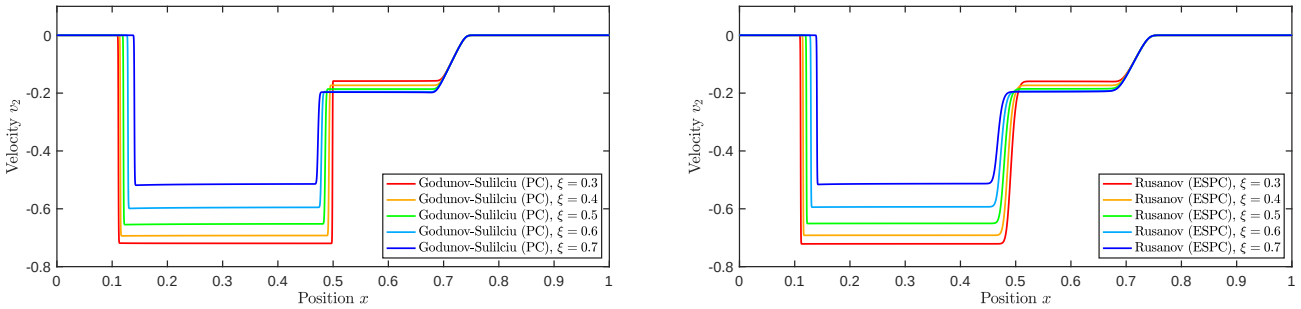

Figure 8: Different phasic mixtures ξ for the *mixture at rest* problem at $t_{\max} = 0.2$ using 16 000 cells. The results for the phasic velocity v_2 are shown, using the (left) Godunov Suliciu (PC) scheme, and the (right) Rusanov (ESPC) scheme.

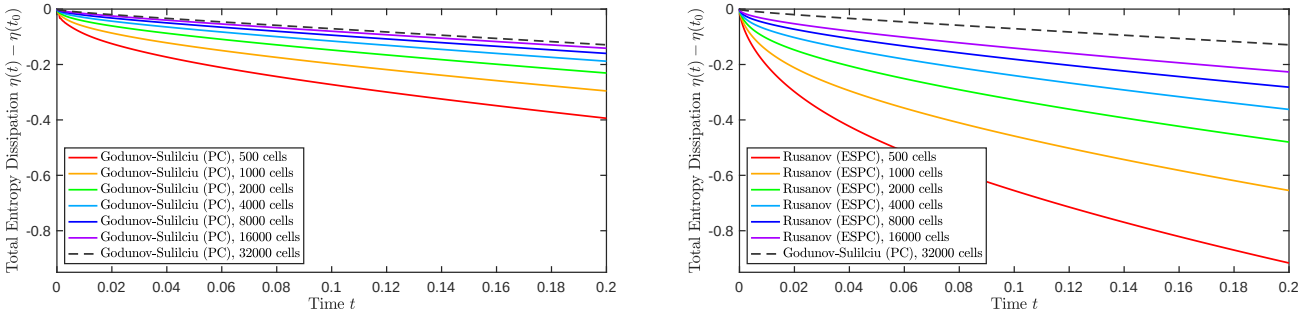

Figure 9: Total entropy dissipation for the *mixture at rest* problem at $t_{\max} = 0.2$ using $\xi = 0.5$ and 16 000 cells. The results for the phasic velocity v_2 are shown, using the (left) Godunov Suliciu (PC) scheme, and the (right) Rusanov (ESPC) scheme.

5.4. *Water faucet problem*

The test case of a *water faucet* was performed by Ransom [41] to investigate the influence of source terms on the mixture of water (indexed by 1) and air (indexed by 2). The source terms are mainly influenced by gravitation,

$$\mathbf{s}(\mathbf{u}) = \begin{pmatrix} \frac{1}{\theta}\frac{\alpha_1\alpha_2}{p_1+p_2}(p_1-p_2) \\ 0 \\ \alpha_1\rho_1 g \\ \alpha_1\rho_1 v_1 g - \frac{1}{\theta}\frac{\alpha_1\alpha_2}{p_1+p_2}(p_1-p_2)p_\mathrm{i} \\ 0 \\ \alpha_2\rho_2 g \\ \alpha_2\rho_2 v_2 g + \frac{1}{\theta}\frac{\alpha_1\alpha_2}{p_1+p_2}(p_1-p_2)p_\mathrm{i} \end{pmatrix}, \tag{55}$$

with gravity $g = 9.81\mathrm{m/s}^2$ and pressure relaxation $\theta = 5 \cdot 10^{-4}$. Initially, we have homogeneous values throughout the vertical tube of 12 m length (which corresponds to a closed water faucet at the end of the tube). With the start of the simulation the water faucet is opened, such that the gravity field is introduced to the problem. The top boundary ($x = 0$) has the same values as the initial values, where the bottom ($x = 12$) of the tube is open to atmospheric conditions [16], see Table 5.

	α_1	ρ_1	v_1	p_1	ρ_2	v_2	p_2
Initial	0.8	1000	10	10^5	1	0	10^5
Top boundary	0.8	1000	10	10^5	1	0	10^5
Bottom boundary	–	–	–	10^5	–	–	10^5

Table 5: Initial and boundary values for the *water faucet* problem.

The interfacial modeling parameter is chosen as $\xi = 0.5$. As closure, ideal gas with $\gamma_1 = 1.0005$, $\gamma_2 = 1.4$, and $c_{\mathrm{v}_1} = c_{\mathrm{v}_2} = 718\ \mathrm{J/kg\,K}$ is chosen [13]. The simulation time is $t_{\max} = 0.5$ sec.

In the following Figure 10 grid refinement results for the air volume fraction α_2 are shown, using the approximate Godunov-Suliciu (PC) solver and the Rusanov (ESPC) solver. It can be seen that both methods converge to the reference solution, while again the entropy-stable scheme converges slower than the relaxation scheme. While the Godunov-Suliciu (PC) solver already shows good agreement with the reference solution by using just 300 grid cells, the Rusanov (ESPC) scheme would need 8000 cells instead. This is due to the fact that the entropy-stable scheme is a more dissipative method.

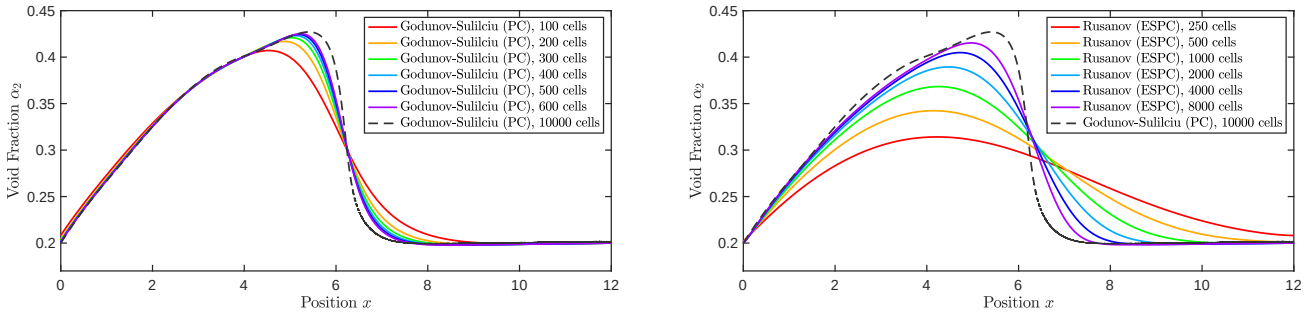

Figure 10: Grid refinement for the *water faucet* problem at $t_{\max} = 0.5$. The results for the air volume fraction α_2 are shown, using the (left) Godunov Suliciu (PC) scheme, and the (right) Rusanov (ESPC) scheme.

5.5. Discussion and analysis of the results

We used four test cases to investigate the qualitative behavior of the Godunov-Suliciu (PC) method and the entropy-stable Rusanov (ESPC) method. With a grid refinement for the *isolated coupling wave* test case we could identify a fast convergence speed of the Godunov-Suliciu (PC) method. Comparing the L_2 norm as the a measure for the accuracy, it can be seen that the Rusanov (ESPC) scheme is more dissipative than the Godunov-Suliciu (PC) scheme. For the *pressure disequilibrium* test case, we investigated the Riemann invariants at the shock of the volume fraction. While the Rusanov (ESPC) scheme not necessarily shows a smooth behavior of the Riemann invariants, in contrast, the Godunov-Suliciu (PC) scheme fulfills at least six of eight Rankine-Hugoniot conditions at the v_{i}-contact discontinuity. By investigating the total entropy dissipation for the *mixture at rest* test case, the Rusanov (ESPC) scheme behaves according to its entropy stable property. But also the Godunov-Suliciu (PC) dissipates entropy with a high convergence rate. For the test cases with source terms, the *water faucet* problem, it was observed that the Rusanov (ESPC) scheme needs a finer mesh than the approximate Godunov-Suliciu (PC) scheme.

6. Conclusion

Within this work a two-velocity two-pressure seven-equations model is developed, which considers important mathematical and thermodynamic properties. As the model only describes transport effects, it is formulated as hyperbolic system by using the non-resonance condition. To preserve the volume fraction α_1 through the v_{i}-contact discontinuity, v_{i} is chosen in such a way that this discontinuity is associated with a linearly degenerate field. Furthermore, the the entropy inequality is derived and used as additional condition, to satisfy the second law of thermodynamics which ensures a physically relevant entropy solution.

The developed inhomogeneous model is in non-conservative form. An approximate Godunov-Suliciu approach is developed to solve the non-conservative parts of the PDE system. As the pressure is non-linear, the conventional model provides genuinely nonlinear waves. Ti find the Riemann invariants we follow the relaxation approach of Suliciu and adapt it to the two-phase flow problem. Due to the non-linearities of the v_{i}-Riemann invariants, the intermediate states of the Riemann problem are difficult to determine. An approximate solution is obtained by weaken the nonlinear Rankine-Hugoniot conditions at the v_{i}-contact discontinuity, such that at least six out of eight original conditions are always fulfilled.

The new scheme is tested with four multiphase flow problems from literature and compared against an entropy-stable Rusanov scheme. Both schemes converge for a grid refinement and dissipate entropy. The approximate Godunov-Suliciu is faster and more accurate than the entropy-stable scheme. Furthermore, it shows a smooth behavior of the Riemann invariants at the shock of the volume fraction.

It is interesting to see that the entropy-stable Rusanov scheme has jumps in every Riemann invariant. It may be that the chosen uniform viscosity for (36) is not the best choice for this problem. For these types of schemes it remains to investigate different viscosity term in order to obtain stable schemes.

Altogether, the here-in developed approximate path-conservative Godunov-Suliciu schemes delivers promising results for the seven-equations two-phase flow model.

Acknowledgments

P. Richter acknowledges funding by the Friedrich-Naumann-Stiftung für die Freiheit, and thanks Martin Frank and Manuel Castro for the discussions.

References

[1] G. Wallis, One-dimensional two-phase flow, McGraw-Hill, 1969.

[2] S. Sahoo, S. Singh, R. Banerjee, Steady state hydrothermal analysis of the absorber tubes used in linear fresnel reflector solar thermal system, Solar Energy 87 (2013) 84–95.

[3] J. Feldhoff, Analysis of once-through boiler concepts in parabolic troughs, Ph.D. thesis, RWTH Aachen University (2015).

[4] J. Feldhoff, T. Hirsch, L. Pitz-Paal, R.and Valenzuela, Transient models and characteristics of once-through line focus systems, Energy Procedia 69 (2015) 626–637.

[5] A. Aurousseau, V. Vuillerme, J.-J. Bezian, Modeling of linear concentrating solar power using direct steam generation with parabolic-trough, in: Proceedings of the 11th International Modelica Conference, Versailles, France, September 21-23, 2015, Vol. 118, Linköping University Electronic Press, 2015, pp. 595–603.

[6] J. Collier, Convective boiling and condensation, McGraw-Hill, 1981.

[7] J. Serrano-Aguilera, L. Valenzuela, Transient validation of relap5 model with the diss facility in once through operation mode, in: SOLARPACES 2015: International Conference on Concentrating Solar Power and Chemical Energy Systems, Vol. 1734, AIP Publishing, 2016, p. 040006.

[8] S. Sahoo, S. Singh, R. Banerjee, Thermal hydraulic simulation of absorber tubes in linear fresnel reflector solar thermal system using relap, Renewable Energy 86 (2016) 507–516.

[9] R. Saurel, R. Abgrall, A multiphase godunov method for compressible multifluid and multiphase flows, Journal of Computational Physics 150 (2) (1999) 425–467.

[10] M. Baer, J. Nunziato, A two-phase mixture theory for the deflagration-to-detonation transition (ddt) in reactive granular materials, International Journal of Multiphase Flow 12 (6) (1986) 861–889.

[11] D. Drew, S. Passman, Theory of Multicomponent Fluids, Applied mathematical sciences, Springer, 1998.

[12] H. Städtke, G. Franchello, B. Worth, Numerical simulation of two-phase flows with stiff source terms, in: Computational Fluid Dynamics 2000, Springer, 2001, pp. 633–638.

[13] A. Ambroso, C. Chalons, P.-A. Raviart, A godunov-type method for the seven-equation model of compressible two-phase flow, Computers & Fluids 54 (2012) 67–91.

[14] N. Andrianov, Analytical and numerical investigation of two-phase flows, Ph.D. thesis, Otto-von-Guericke-Universität Magdeburg, Universitätsbibliothek (2003).

[15] S. Müller, M. Hantke, P. Richter, Closure conditions for non-equilibrium multi-component models, Continuum Mechanics and Thermodynamics 28 (4) (2015) 1157–1189.

[16] T. Gallouët, J.-M. Hérard, N. Seguin, Numerical modeling of two-phase flows using the two-fluid two-pressure approach, Mathematical Models and Methods in Applied Sciences 14 (05) (2004) 663–700.

[17] F. Coquel, J.-M. Hérard, K. Saleh, N. Seguin, Two properties of two-velocity two-pressure models for two-phase flows, Communications in Mathematical Sciences 12 (3).

[18] P. Richter, Simulation and optimization of solar thermal power plants, Ph.D. thesis, RWTH Aachen University (2017).

[19] A. Harten, High resolution schemes for hyperbolic conservation laws, Journal of computational physics 49 (3) (1983) 357–393.

[20] K. Saleh, Analyse et simulation numérique par relaxation d'ecoulements diphasiques compressibles. contribution au traitement des phases evanescentes., Ph.D. thesis, Université Pierre et Marie Curie-Paris VI (2012).

[21] J.-M. Hérard, A three-phase flow model, Mathematical and computer modelling 45 (5) (2007) 732–755.

[22] R. LeVeque, Numerical Methods for Conservation Laws, Lectures in Mathematics ETH Zürich, Department of Mathematics Research Institute of Mathematics, Springer, 1992.
URL `http://books.google.de/books?id=3WhqLPcMdPsC`

[23] E. Tadmor, The numerical viscosity of entropy stable schemes for systems of conservation laws. i, Mathematics of Computation 49 (179) (1987) 91–103.

[24] E. Godlewski, P.-A. Raviart, Numerical approximation of hyperbolic systems of conservation laws, Vol. 118, Springer, 1996.

[25] C. Parés, M. Muñoz-Ruiz, On some difficulties of the numerical approximation of nonconservative hyperbolic systems, Bol. Soc. Esp. Mat. Apl 47 (47) (2009) 23–52.

[26] C. Parés, Numerical methods for nonconservative hyperbolic systems: a theoretical framework., SIAM Journal on Numerical Analysis 44 (1) (2006) 300–321.

[27] M. Castro, U. Fjordholm, S. Mishra, C. Parés, Entropy conservative and entropy stable schemes for nonconservative hyperbolic systems, SIAM Journal on Numerical Analysis 51 (3) (2013) 1371–1391.

[28] G. Dal Maso, P. G. LeFloch, F. Murat, Definition and weak stability of nonconservative products, J. Math. Pures Appl., IX. Sér. 74 (6) (1995) 483–548.

[29] R. Abgrall, S. Karni, A comment on the computation of non-conservative products, Journal of Computational Physics 229 (8) (2010) 2759–2763.

[30] A. Canestrelli, A. Siviglia, M. Dumbser, E. F. Toro, Well-balanced high-order centred schemes for non-conservative hyperbolic systems. Applications to shallow water equations with fixed and mobile bed, Advances in Water Resources 32 (6) (2009) 834–844.

[31] R. LeVeque, Finite volume methods for hyperbolic problems, Vol. 31, Cambridge University Press, 2002.

[32] M. Castro, P. LeFloch, M. Muñoz-Ruiz, C. Parés, Why many theories of shock waves are necessary: Convergence error in formally path-consistent schemes, Journal of Computational Physics 227 (17) (2008) 8107–8129.

[33] U. Fjordholm, S. Mishra, Accurate numerical discretizations of non-conservative hyperbolic systems, ESAIM: Mathematical Modelling and Numerical Analysis 46 (01) (2012) 187–206.

[34] D. Serre, Systemes de lois de conservation. I. Hyperbolicité, entropies, ondes de choc. Fondations, Diderot Editeur, Paris, 1996.

[35] I. Suliciu, On modelling phase transitions by means of rate-type constitutive equations. shock wave structure, International Journal of Engineering Science 28 (8) (1990) 829–841.

[36] I. Suliciu, On the thermodynamics of fluids with relaxation and phase transitions. fluids with relaxation, Int. J. Engag. Sci 36 (1998) 921–947.

[37] T. Flåtten, H. Lund, Relaxation two-phase flow models and the subcharacteristic condition, Mathematical Models and Methods in Applied Sciences 21 (12) (2011) 2379–2407.

[38] G. Whitham, Linear and Nonlinear Waves, John Wiley & Sons, 1974.

[39] T.-P. Liu, Hyperbolic conservation laws with relaxation, Communications in Mathematical Physics 108 (1) (1987) 153–175.

[40] D. Schwendeman, C. Wahle, A. Kapila, The riemann problem and a high-resolution godunov method for a model of compressible two-phase flow, Journal of Computational Physics 212 (2) (2006) 490–526.

[41] V. Ransom, Numerical benchmark tests, Multiphase Science and Technology 3 (1-4).